Optical tweezer measurements of asymptotic nonlinearities in complex fluids

Satish Kumar Gupta,[1] Kyle R. Lennon,[2] Mary A. Joens,[2] Hari Bandi,[3] Martijn Van Galen,[4] YuLong Han,[1] Wenhui Tang,[1] Yiwei Li,[1] Steven Charles Wasserman,[5] James W. Swan,[2] and Ming Guo[1,*]

[1]*Department of Mechanical Engineering, Massachusetts Institute of Technology, Cambridge, Massachusetts 02139, USA*
[2]*Department of Chemical Engineering, Massachusetts Institute of Technology, Cambridge, Massachusetts 02139, USA*
[3]*Operations Research Center, Massachusetts Institute of Technology, Cambridge, Massachusetts 02139, USA*
[4]*Physical Chemistry and Soft Matter, Wageningen University & Research, NL-6708 WE Wageningen, The Netherlands*
[5]*Department of Biological Engineering, Massachusetts Institute of Technology, Cambridge, Massachusetts 02139, USA*

(Received 13 May 2021; accepted 11 November 2021; published 7 December 2021)

This article presents micro-medium-amplitude oscillatory shear (μMAOS), a method to measure the frequency-dependent micromechanical properties of soft materials in the asymptotically nonlinear regime using optical tweezers. We have developed a theoretical framework to extract these nonlinear mechanical properties of the material from experimental measurements and also proposed a physical interpretation of the third-order nonlinearities measured in single-tone oscillatory tests. We validate the method using a well-characterized surfactant solution of wormlike micelles, and subsequently employ this technique to demonstrate that the cytoplasm of a living cell undergoes strain softening and shear thinning when locally subjected to weakly nonlinear oscillatory deformations.

DOI: 10.1103/PhysRevE.104.064604

I. INTRODUCTION

Active microrheology has emerged as a canonical method for micromechanical characterization of soft materials that is important in several applications, such as food science [1], tissue engineering [2], regenerative medicine [3], wearable electronics [4], and pharmaceuticals [5]. The several advantages of these micromechanical measurements over bulk rheology include a wide- and high-frequency bandwidth for probing viscoelasticity, local probing for heteregenous and multiphase systems, and small required sample volumes [6,7]. Microrheological measurements are often made in the linear viscoelastic regime or under steady flow conditions [8–10]; however, many soft materials exhibit a nonlinear viscoelastic response during modest unsteady deformations, a behavior not characterized by linear or steady flow tests.

Recently, several time-dependent nonlinear microrheological tests have been developed in analog to bulk rheological techniques, including optically driven microscopic step-stress experiments [11], as well as the start-up, cessation, and periodic reversal of the steady translation of an optically trapped bead [12–14]. All of these methods probe either steady or transient features of the viscoelastic response of the surrounding matrix. Other bulk nonlinear tests do not yet have a direct microrheological analog, including spectral methods such as large and medium amplitude oscillatory shear tests, which characterize the nonlinear frequency-dependent behavior of soft materials using sinusoidal deformations [15–20]. Thus, the microscopic equivalents of these feature-rich, frequency-dependent nonlinear material properties have not been directly accessed by any existing microrheological technique.

In this article, we develop the microscopic counterpart to the medium amplitude oscillatory shear (MAOS) test using optical tweezers, henceforth referred to as micro-MAOS, or μMAOS (Fig. 1). This μMAOS framework represents the first spectral microrheological technique for studying the nonlinear response of viscoelastic materials. For optical tweezers active microrheology in the linear regime, the procedure for isolating the dynamic mechanical properties of the material from the characteristics of the optical trap is well known [21–25]. However, this procedure is no longer valid when probing nonlinear mechanics. Through μMAOS, we obtain nonlinear viscoelastic properties that are independent of the strength of the optical trap by applying the Volterra series expansion to the general relationship between the resistive force exerted by the material on the probe bead and the velocity of the bead [26]. Furthermore, we also provide a physical interpretation of the third-order nonlinearities observed in single-tone oscillatory microrheological tests (Fig. 2).

The following section presents a mathematical derivation of the μMAOS framework, including our proposed interpretation of the weak nonlinearities measured by single-frequency μMAOS experiments. We follow this discussion with a brief description of the experimental methods in Sec. III. The experimental protocol and mathematical framework of μMAOS is then applied to four fluids: a Newtonian solution of glycerol in water, a well-characterized viscoelastic solution composed of wormlike micelles, the cytoplasm of a living mammalian cell, and an entangled network of linear polymers. These four studies validate the applicability of μMAOS to a variety of fluids with different phenomenology, and demonstrate how our proposed framework can be used to elucidate previously

*guom@mit.edu

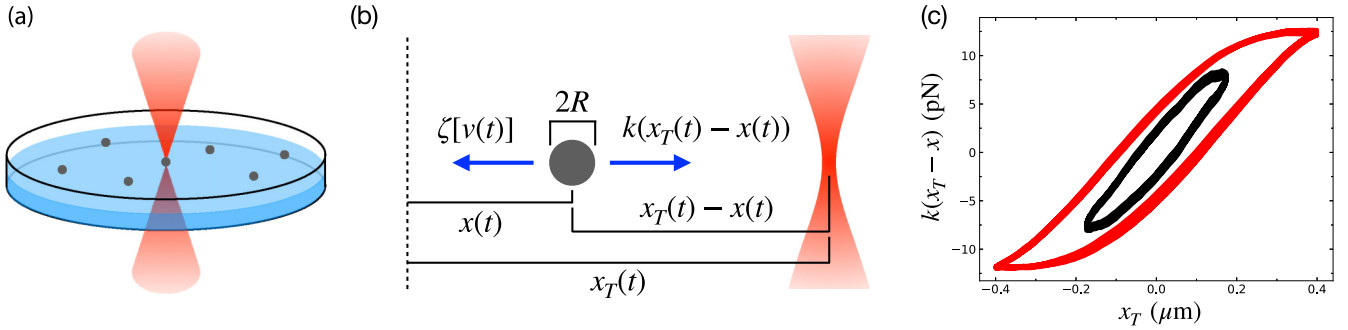

FIG. 1. Schematic representation of nonlinear micromechanical measurements via optical tweezers. (a) Bead within the soft material trapped by optical tweezers (not to scale). (b) Depiction of the trapping and mechanical forces in the system. (c) Trapping force vs trap displacement curves showing linear and nonlinear mechanical behavior at amplitudes of 0.175 and 0.4 μm, respectively, at 500 rad/s for a 5 wt% aqueous PEO solution.

unknown features of the nonlinear dynamical response of complex fluids.

II. MATHEMATICS OF μMAOS

We study the asymptotically nonlinear—or medium amplitude—regime because it is difficult to define material functions for arbitrarily large amplitude oscillatory tests, where an unbounded number of higher harmonics emerge. Moreover, very large amplitudes are inaccessible for many materials, as a number of experimental and physical artifacts are observed in this regime [19]. Alternatively, medium amplitude tests provide distinct information from linear tests, but avoid the data abstraction and experimental artifacts of large amplitude tests.

A schematic of our experimental system is shown in Fig. 1. It consists of a spherical submicron-sized bead immersed in a soft material. The bead is trapped by optical tweezers, which are manipulated by a set of acousto-optic deflectors according to some time-varying, user-supplied protocol. When the trap created by the optical tweezers is displaced from the center of the bead, it exerts a springlike restoring force that pulls the bead towards the focus of the trap. This force is balanced by the resistance supplied by the surrounding medium, and the inertia of the bead. In the low-Reynolds number limit, inertia is negligible, and the resistance exactly balances the trapping force. In the Hookean limit of the trapping force (i.e., for small displacements of the trap from the bead) we express this force balance as

$$0 = -\zeta[v(t)] - k(x(t) - x_T(t)). \tag{1}$$

Here, $x(t)$ and $v(t)$ represent the position and velocity of the bead, and $x_T(t)$ represents the focus of the trap. The mechanical force exerted on the bead by the surrounding medium is $\zeta[v(t)]$, which is a nonlinear, material-specific functional of $v(t)$. In bulk rheometry, it is common to measure analogous properties using oscillatory protocols, which we extend to microrheology here. For oscillatory experiments, it is convenient to employ the Fourier transform of the force balance:

$$0 = -\zeta^*[i\omega\hat{x}(\omega)] - k(\hat{x}(\omega) - \hat{x}_T(\omega)). \tag{2}$$

We now represent the particle and trap positions in terms of their Fourier transforms, denoted by carets: $\hat{x}(\omega)$ and $\hat{x}_T(\omega)$. This transformation allows us to rewrite the transformed particle velocity in terms of the transformed particle position: $\hat{v}(\omega) = i\omega\hat{x}(\omega)$.

For isotropic materials, the functional $\zeta^*[i\omega\hat{x}(\omega)]$ exhibits odd symmetry with respect to $\hat{v}(\omega)$ due to frame invariance of the force balance, with the following frequency-domain Volterra series expansion:

$$\zeta^*[i\omega\hat{x}(\omega)] = \sum_{n\in\text{odds}} \frac{1}{(2\pi)^{n-1}} \int \cdots \int_{-\infty}^{\infty} \zeta_n^*(\omega_1, \cdots, \omega_n) \times \delta\left(\omega - \sum_{m=1}^{n} \omega_m\right) \prod_{m=1}^{n} i\omega_m \hat{x}(\omega_m) d\omega_m. \tag{3}$$

The transfer functions $\zeta_n^*(\omega_1, \cdot, \omega_n)$ are the material-specific properties characterized by oscillatory microrheological experiments, and we define the medium amplitude regime as that wherein only the first two terms of this Volterra series are resolvable above the experimental noise [15,16]. For a spherical bead with radius R, the linear transfer function is directly proportional to the complex viscosity, $\eta^*(\omega) = G^*(\omega)/(i\omega) = \zeta_1^*(\omega)/(6\pi R)$. The product of the third-order transfer function $\zeta_3^*(\omega_1, \omega_2, \omega_3)$ and the bead radius R represents a newly defined, nonlinear material property that has not been measured directly in any previous microrheological study. Measuring this transfer function is the primary objective of μMAOS.

Equations (2) and (3) are not yet sufficient to compute $\zeta_1^*(\omega)$ and $\zeta_3^*(\omega_1, \omega_2, \omega_3)$ from μMAOS data, because the

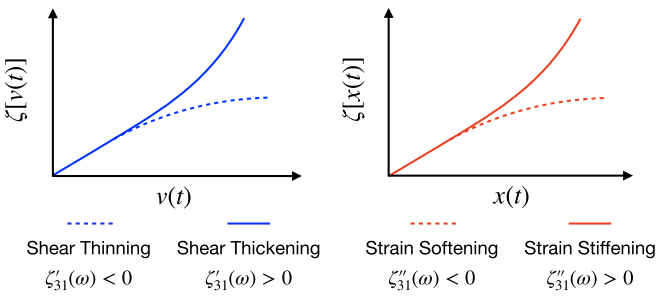

FIG. 2. Physical interpretation of the sign of the third-order, first harmonic nonlinear response for the limiting cases of purely viscous (left) and purely elastic materials (right).

particle position $\hat{x}(\omega)$ appears inside the Volterra series but is not a directly controlled quantity. In optical tweezers active microrheology, measurements proceed by controlling $\hat{x}_T(\omega)$ and measuring $\Delta(\omega) = \hat{x}_T(\omega) - \hat{x}(\omega)$ with a quadrant photodiode [21]. Therefore, we define an alternate Volterra series directly relating the experimental input and output:

$$\Delta(\omega) = \sum_{n\in\text{odds}} \frac{1}{(2\pi)^{n-1}} \int \cdot \int_{-\infty}^{\infty} R_n^*(\omega_1, \cdot, \omega_n) \times \delta(\omega - \sum_{m=1}^{n} \omega_m) \prod_{m=1}^{n} \hat{x}_T(\omega_m) d\omega_m. \quad (4)$$

If we define a characteristic amplitude A for variations in the trap position, then the transfer functions $R_n^*(\omega_1, \cdot, \omega_n)$ can be inferred directly from data at different A using polynomial regression. This inference is performed by the MITMAPS software package adapted from [17]. By comparing Eq. (4) to Eqs. (2) and (3), we obtain equations relating the measured transfer functions $R_1^*(\omega)$ and $R_3^*(\omega_1, \omega_2, \omega_3)$ to the linear and medium amplitude material transfer functions [27]:

$$\zeta_1^*(\omega) = \frac{kR_1^*(\omega)}{i\omega[1 - R_1^*(\omega)]}, \quad (5)$$

$$\zeta_3^*(\omega_1, \omega_2, \omega_3) = \frac{kR_3^*(\omega_1, \omega_2, \omega_3)}{[1 - R_1^*(\Omega)] \prod_{j=1}^{3} i\omega_j [1 - R_1^*(\omega_j)]}, \quad (6)$$

with $\Omega = \omega_1 + \omega_2 + \omega_3$. These expressions allow us to directly relate active microrheological data to weakly nonlinear material properties.

The mathematical development herein has so far been independent of some specific driving function $x_T(t)$ [16]. For the sake of simplicity, however, we now restrict our attention to single-tone drives of the form $x_T(t) = A\sin(\omega_0 t)$, where A and ω_0 are the amplitude and angular frequency of the trap oscillations, respectively. Substituting the single-tone signal into Eqs. (4)–(6), we find that a weakly nonlinear single-tone drive elicits both a linear and third-order material response at the driving frequency (ω_0), and a purely third-order response at the third harmonic ($3\omega_0$). The coefficient weighting the linear response at ω_0 is the linear transfer function $\zeta_1^*(\omega_0)$. The coefficients weighting the third-order response elements are certain values of the third-order transfer function:

$$\zeta_3^*(\omega_0, -\omega_0, \omega_0) \equiv \zeta_{31}^*(\omega_0) = \zeta_{31}'(\omega_0) - i\zeta_{31}''(\omega_0), \quad (7a)$$

$$\zeta_3^*(\omega_0, \omega_0, \omega_0) \equiv \zeta_{33}^*(\omega_0) = \zeta_{33}'(\omega_0) - i\zeta_{33}''(\omega_0). \quad (7b)$$

Here, $\zeta_{31}^*(\omega)$ and $\zeta_{33}^*(\omega)$ describe the first and third harmonic nonlinearity, respectively. It is common to interpret the real and imaginary components of the linear complex viscosity, $\eta^*(\omega) = \eta'(\omega) - i\eta''(\omega)$, as representing viscous and elastic components of the linear response, respectively. We may extend this interpretation to the nonlinear properties, where $\zeta_{31}'(\omega)$ ($\zeta_{33}'(\omega)$) represents a viscous nonlinearity and $\zeta_{31}''(\omega)$ ($\zeta_{33}''(\omega)$) represents an elastic nonlinearity on the first (third) harmonic.

Unlike $\eta'(\omega)$ and $\eta''(\omega)$, the real and imaginary components of the nonlinear properties can be either positive or negative, and we may interpret their signs in terms of the mechanical properties of our material. To develop this interpretation, it is instructive to consider some limiting examples. For a purely viscous medium in the linear regime, the mechanical force $\zeta[v(t)]$ responds proportionally to $v(t)$. For nonlinear deformations, however, this curve may bend downwards or upwards, corresponding to shear thinning or shear thickening, respectively. Asymptotically, this curvature is dictated by the sign of the real component of the first harmonic nonlinearity $\zeta_{31}'(\omega)$, with $\zeta_{31}'(\omega) < 0$ corresponding to shear thinning and $\zeta_{31}' > 0$ corresponding to shear thickening. Similarly, for a purely elastic medium in the linear regime, the mechanical force $\zeta[x(t)]$ responds proportionally to $x(t)$. In the nonlinear regime, negative curvature ($\zeta_{31}'' < 0$) in this relationship corresponds to strain softening and positive curvature ($\zeta_{31}'' > 0$) to strain stiffening. Figure 2 depicts these limiting cases. For a viscoelastic material, the mechanical force is no longer dictated instantaneously by either $v(t)$ or $x(t)$, and plots of $\zeta[v(t)]$ against either $v(t)$ or $x(t)$ for oscillatory probes will look like deformed ellipses [e.g., the red curve in Fig. 1(c)]. However, $\zeta_{31}'(\omega)$ and $\zeta_{31}''(\omega)$ still provide information about curvature in the deformed ellipses, and their signs can be associated with average shear thinning/thickening and strain softening/stiffening over one period of oscillation [15].

III. EXPERIMENTAL METHODS

A. Materials

1. Polystyrene probe particles

Throughout all experiments in this article, we use fluorescent carboxylate-modified polystyrene latex beads with radius $R = 0.44$ μm (from Molecular Probes) as probe particles, which are small enough to maneuver inside of the cytoplasm but substantially larger than the characteristic mesh size for each material studied in this work [28–31]. These particles are rendered inert by grafting short amine-terminated methoxy-poly(ethylene glycol) to their surface, as described previously [32]. These grafts limit surface interactions with the viscoelastic matrix, particularly cytoplasmic proteins [33,34], which is critical for ensuring that the experiments measure the continuum viscoelastic properties of the surrounding matrix. These inert particles are stored at 4°C and used within two weeks.

2. Wormlike micellar solution

The surfactant solution of wormlike micelles used in this study was composed of cetylpyridinium chloride (CPyCl), sodium salicylate (NaSal), and sodium chloride (NaCl) in de-ionized water at concentrations of 100 mM, 60 mM, and 33 mM, respectively (CPyCl and NaSal supplied by Alfa Aesar; reagent grade NaCl purchased from Sigma Aldrich).

3. Cell cultures and microinjection

Mouse embryonic fibroblasts (mEFs) [35] were cultured in Dulbecco's minimal essential medium (Corning, NY) supplemented with 10% fetal calf serum (Gibco, Life Technologies, Gaithersburg, MD) and 1% penicillin-streptomycin (Gibco, Life Technologies, Gaithersburg, MD) at 37°C and 5% CO2 in humid conditions. Cells were transferred onto 35-mm micropatterned dishes and allowed to grow overnight. Microinjection of probe particles was performed using a glass needle and a FemtoJet microinjector (Eppendorf) mounted on a bright-field microscope. About 50 cells were injected per

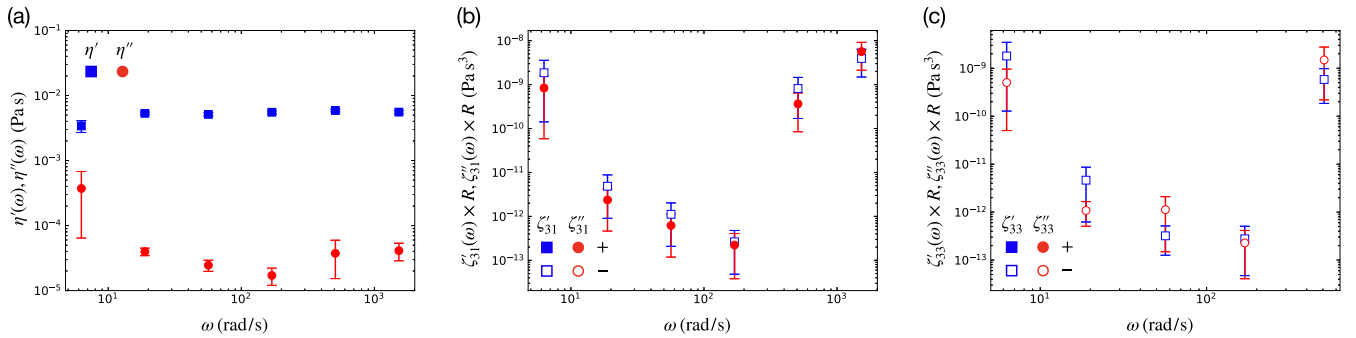

FIG. 3. Validation of μMAOS framework for a Newtonian fluid (a 50 wt% aqueous glycerol solution). (a) The real and imaginary components $\eta'(\omega)$ and $\eta''(\omega)$ of the linear complex viscosity obtained from μMAOS measurements. (b) and (c) The third-order material properties $\zeta'_{31}(\omega)$, $\zeta''_{31}(\omega)$, $\zeta'_{33}(\omega)$, and $\zeta''_{33}(\omega)$ obtained from μMAOS measurements, depicted with filled and unfilled symbols to indicate where data are positive and negative, respectively. Data represent the average over 20 trials, with error bars representing one standard error uncertainty.

dish; each cell was injected with up to 50 tracer particles to eliminate the interference to cell function. Cells were then allowed to recover in culture medium for 6 h before the μMAOS measurements were performed.

B. μMAOS experimental protocol

The beam from a single-mode continuous wave (CW) Ytterbium fiber laser (10 W, 1064 nm; IPG Photonics, MA) is directed through a series of Keplerian beam expanders to overfill the back aperture of a 1.45 numerical aperture microscope objective (CFI Plan Apo Lambda DM 100X Oil; Nikon Corp., Japan), which focuses the beam to optically trap and manipulate the probe beads immersed in viscoelastic media. Two-axis acousto-optic deflectors (IntraAction Corp., IL) are used to maneuver the beam in the plane of the microscope glass slide and subsequently manipulate the trapped bead. To measure the position of the probe, the bead is centered on a high-resolution position detection quadrant detector (Thorlabs Inc., NJ) with brightfield illumination from a 100-W lamp.

The linear region of the detector was previously calibrated by trapping a bead identical to those used in this article and moving it across the detector using the acousto-optic deflectors in known step sizes. The trap stiffness was calibrated using the mean-squared Brownian motion of a trapped bead in solution of glycerol and water at various laser power densities using the principle of energy equipartition [36]. Due to the slightly different indices of refraction in the cellular cytoplasm and water, we use a water/glycerol solution with a matched index of refraction to calibrate the trap for the measurements in cells.

Finally, to perform the μMAOS experiments described herein, the optical trap is subjected to sinusoidal oscillations at six logarithmically spaced frequencies between 6.28 and 1526 rad/s, with measurements at 12 amplitudes spaced linearly between 0.175 and 0.45 $\mu\mu$m, and the laser position and bead displacement are recorded simultaneously. These amplitudes were selected to ensure that the distance between the particle and trap, Δ, is sufficiently described by a cubic polynomial in the trap position. The largest of these amplitudes is nearly equal to a single particle radius, therefore the focus of the trap never exceeds a single particle diameter of separation from the probe, ensuring that bead dropout will not hamper the microrheological tests. The absence of dropout can be verified visually in Fig. 1(c), which shows that the force-displacement curve for even a high-amplitude experiment in polyethylene oxide varies gradually, without any sudden changes characteristic of dropout.

IV. RESULTS

A. Glycerol-Water solution

To validate the applicability of the μMAOS protocol in the linear limit, and to verify the linearity of the instrumental tools, we first study the mechanical response of a 50 wt% solution of glycerol in water. The measurements in glycerol faithfully reproduce the expected Newtonian viscosity of the solution [Fig. 3(a)] indicating proper calibration of the equipment. Moreover, the nonlinear response detected in glycerol is nearly 10 orders of magnitude less than those measured in viscoelastic solutions [Figs. 3(b) and 3(c)], suggesting that nonlinearities due to the detection and trapping mechanisms, including highly nonlinear effects such as the bead dropping out of the optical trap, have negligible impact on our measurements.

B. Wormlike micellar solution

We next apply μMAOS to a well-characterized wormlike micellar solution—100:60:33 mM CPyCl:NaSal:NaCl in deionized water—to validate the scheme in the medium amplitude regime. First, we compare the complex moduli obtained from the μMAOS technique to predictions of the corotational Maxwell (CRM) model:

$$\lambda \frac{\mathcal{D}\boldsymbol{\tau}_p}{\mathcal{D}t} + \boldsymbol{\tau}_p = \eta_p(\nabla \mathbf{u} + (\nabla \mathbf{u})^T), \tag{8}$$

with a relaxation time spectrum described by a single discrete relaxation mode plus a continuous spectrum of fast-relaxing Rouse dynamics:

$$P(\lambda) = \frac{(1-B)e^{-\lambda/\lambda_c}}{\sqrt{\pi \lambda_c \lambda}} + B\delta(\lambda - \lambda_p). \tag{9}$$

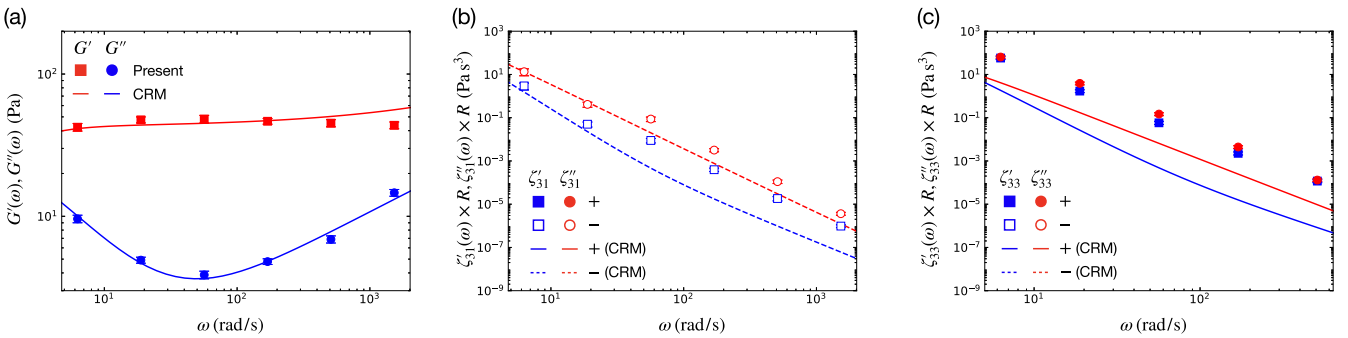

FIG. 4. Validation of the μMAOS framework using a CPyCl wormlike micellar solution. (a) The elastic and viscous moduli, $G'(\omega)$ and $G''(\omega)$, obtained from μMAOS measurements. (b) and (c) The third-order material properties, $\zeta'_{31}(\omega)$, $\zeta''_{31}(\omega)$, $\zeta'_{33}(\omega)$, and $\zeta''_{33}(\omega)$ obtained from μMAOS measurements, depicted with filled and unfilled symbols to indicate where data are positive and negative, respectively. Data represent the average over 20 trials, with error bars representing one standard error uncertainty. Predictions of the corotational Maxwell model with high-frequency Rouse dynamics are depicted with solid and dashed lines to indicate positive and negative values, respectively.

This model has been previously validated to approximate the linear and weakly nonlinear viscoelasticity of this micellar solution using bulk rheological measurements [37], and we similarly observe close agreement between the model and the measured linear response [Fig. 4(a)].

To validate the nonlinear measurements, we compute predictions for $\zeta^*_{31}(\omega)$ and $\zeta^*_{33}(\omega)$ from the CRM model using this relaxation time spectrum [27]. Details regarding these analytical predictions are presented more extensively in [27]. The result shows qualitative agreement between the model predictions and data [Figs. 4(b) and 4(c)]. Without any adjustable parameters to fit the nonlinear response, the model predicts the correct sign for all four nonlinear properties, as well as the approximate magnitude and frequency dependence of the data. This level of agreement is supported by bulk rheological measurements, for which the CRM model also underestimates the magnitude of the weakly nonlinear response [17], likely due to its inability to capture more detailed physical effects of the micellar solution, such as the elongation of micellar segments. Still, that such agreement is observed between our data and a constitutive model known to approximate the mechanical response of this micellar solution in bulk rheometry verifies that μMAOS indeed measures intrinsic nonlinear properties of viscoelastic materials.

C. Mammalian cellular cytoplasm

We finally demonstrate the capability of μMAOS to discern previously unknown physical traits of soft materials by characterizing the nonlinear, time-dependent response of the cytoplasm of a living cell. The mechanical properties of the cytoplasm play important roles in regulating many key cellular physiological functions, such as mechanotransduction [38], cancer metastasis [39], cell signaling [40], and stem cell fate [41,42]. A significant portion of cell mechanics studies are limited to the linear regime [21,22,43,44]. Some studies have examined nonlinear behavior, showing that cells stiffen when subjected to an external stress [36,45,46]. However, these studies externally probe the cell, measuring the rigid actin cortex instead of the cytoplasm [47]. In fact, we know from previous studies that the linear cytoplasmic mechanics is distinct from the cortex, with the latter being two orders of magnitude stiffer [21,42,43,48]. Thus, our goal here is to directly probe the cytoplasm of a living cell to characterize its previously unknown nonlinear behavior, as it could lead to significant insights into how critical physiological processes are mechanically regulated.

We introduce probe beads inside the cytoplasm of mouse embryonic fibroblasts (mEFs) by endocytosis [22]. To avoid effects caused by the cellular cortex, we apply the μMAOS technique only to beads that are at least 1.5 μm from the cortex. From these measurements, we find that the storage and loss moduli in the linear regime [Fig. 5(a)] show weak power-law dependence on frequency with a magnitude ranging from 1 to 30 Pa. These measurements are consistent with previous observations for mammalian cytoplasm [21,33,48], suggesting that both surface interactions between the bead and cytoplasmic proteins and effects from the stiffer cellular cortex are indeed minimal. Both components of the first- and third-harmonic nonlinear properties [Figs. 5(b) and 5(c)] exhibit a $\sim\omega^{-3}$ power-law decay over the measured frequency range, similar to the behavior of the nonlinear properties of the wormlike micellar solution. Thus, the observed behavior is consistent with our expectations for simple viscoelastic materials with fading memory.

The first-harmonic nonlinear properties $\zeta'_{31}(\omega)$ and $\zeta''_{31}(\omega)$ are both negative throughout the measurement window, implying that the cytoplasm exhibits a dynamic strain softening and shear thinning behavior distinct from that of the stress-stiffening cortex. The strain softening of the cytoplasm is possibly due to its relatively sparse filamentous actin compared to the cortex [49] and unbinding of the network due to mechanical disruption, as observed in previous studies [50]. Furthermore, consistent intracellular softening and fluidification behavior of the cytoplasm was observed during cell division [51]. We believe that this behavior aids in intracellular processes within the cytoplasm by providing a soft environment that is distinct from the cortex, which stiffens under external physical stress as a mechanism for protecting the soft cytoplasm.

The observation of dynamic softening of the cytoplasm is supported by recent theoretical studies, which predict shear thinning of the cytoplasm in steady flow [52], and by experimental observations of strain softening of the

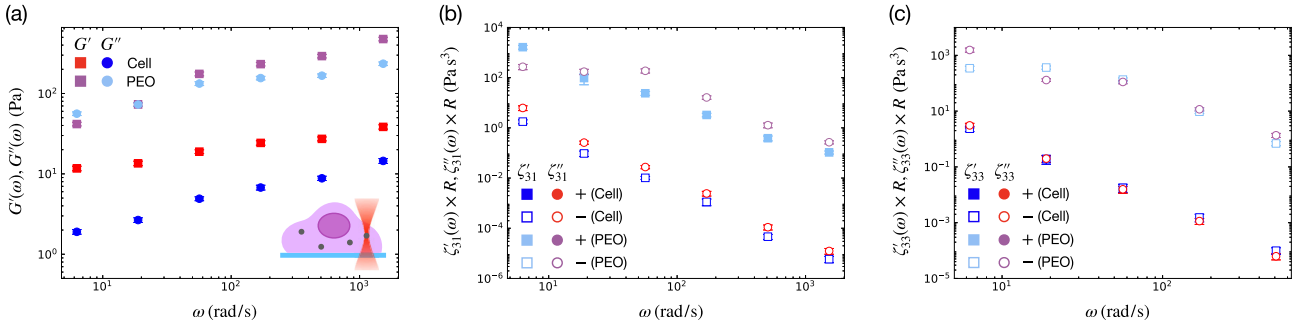

FIG. 5. μMAOS studies of the cytoplasm of a living cell and of an entangled solution of polymers. (a) A schematic of an optically trapped bead within the cellular cytoplasm is shown as an inset. The linear elastic and viscous moduli $G'(\omega)$ and $G''(\omega)$ obtained from μMAOS measurements in the cytoplasm of an mEF cell and in a 5 wt% solution of PEO in water. (b) and (c) The third-order material properties $\zeta'_{31}(\omega)$, $\zeta''_{31}(\omega)$, $\zeta'_{33}(\omega)$, and $\zeta''_{33}(\omega)$ obtained from μMAOS measurements. Data from the mEF cytoplasm are represented by blue and red symbols, while data from PEO are represented with light blue and purple symbols, with filled and unfilled symbols used to denote positive and negative values, respectively. Data represent the average over 20 trials, with error bars representing one standard error uncertainty.

cytoplasm [14] after cyclic steady loading. To further support the observation made from the μMAOS measurements that the mammalian cytoplasm exhibits a dynamic strain softening and shear thinning behavior, and to contrast the mechanics of the mammalian cytoplasm with that of the cellular cortex, we conduct unidirectional dragging experiments both in the cytoplasm and near the cortex. In these experiments, an optically trapped bead is displaced at a steady rate, and the force exerted by the surrounding medium on the bead is measured by observing the displacement between the bead and the optical trap. Otherwise, the experimental setup and protocol is the same as for μMAOS experiments, described in Sec. III B. Figure 6 shows the result of these unidirectional dragging experiments.

Although these experiments capture the nonlinear mechanics of the cytoplasm and cortex only in the steady limit, whereas μMAOS measurements are inherently dynamic and therefore correspond to a finite time scale, these measurements do support the observation that the cytoplasm is strain softening. The strain softening behavior is evident in the negative concavity of the force vs displacement curve, which would correspond to $\zeta''_{31}(\omega) < 0$ in the limit of $\omega \to 0$. The cytoplasm, on the other hand, exhibits a strain stiffening response, corresponding to $\zeta''_{31}(\omega) > 0$ in the limit of $\omega \to 0$. Therefore, the unidirectional dragging experiments support the conclusions made from the μMAOS data that the cytoplasm is strain softening, and that its behavior is distinct from that of the strain stiffening cortex.

D. Polyethylene oxide

The unique capabilities of μMAOS to study the nonlinear mechanical properties of complex fluids at the microscale are further demonstrated by comparing the data from the mEF cytoplasm to that obtained in another material with similar linear viscoelastic characteristics. Figure 5 also presents data taken in an aqueous solution of 5 wt% polyethylene oxide (PEO), a solution which forms a weakly entangled polymeric network that might be considered a surrogate model for the cytoplasm. Indeed, $G'(\omega)$ and $G''(\omega)$ for both the cytoplasm and PEO exhibit weak power-law dependence on frequency [Fig. 5(a)], consistent with previous observations [53].

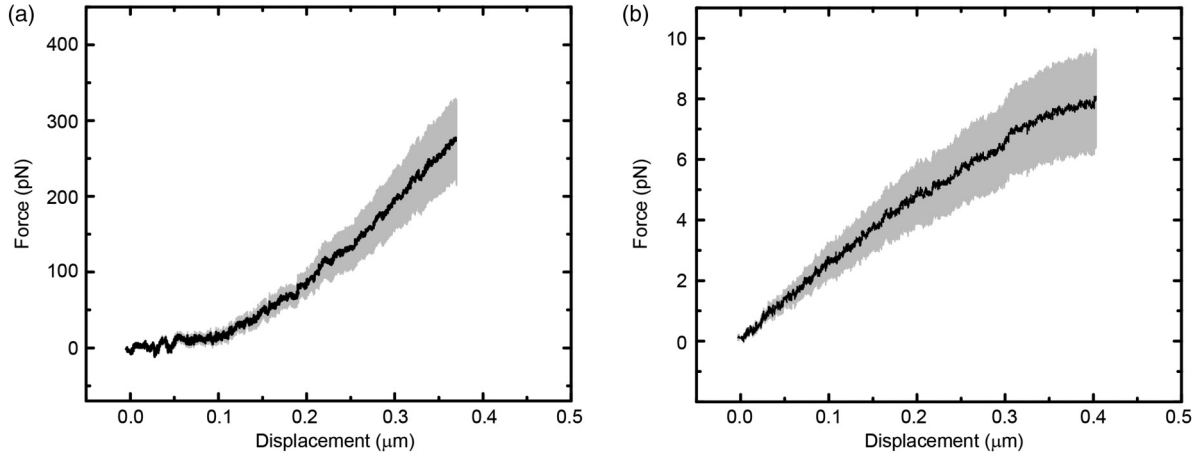

FIG. 6. Unidirectional dragging measurements of an optically trapped bead in a living mammalian cell. (a) Measurements near the cellular cortex, which depict a strain stiffening behavior (positive concavity in the force vs displacement curve). (b) Measurements in the cytoplasm, away from the cortex, which depict a strain softening behavior (negative concavity in the force vs displacement curve). The solid black line corresponds to the mean over 20 trials, and the shaded region corresponds to one standard error of the mean.

However, $\zeta'_{31}(\omega)$ is measured to be positive for PEO but negative for the mEF cytoplasm, indicating that while the cytoplasm is shear thinning in the measured frequency window, the PEO solution is asymptotically shear thickening—an observation supported by bulk rheological measurements of concentrated PEO solutions [54]. With the sensitivity of μMAOS to this nonlinear material property, we are able to distinguish the distinct nonlinear characteristics of two materials with qualitatively similar linear viscoelastic responses.

V. CONCLUSION

This article demonstrates that μMAOS sensitively probes aspects of soft material physics that are difficult, or impossible, to ascertain using other methods. Despite the mathematical complexity of μMAOS compared to linear microrheology, conducting μMAOS experiments does not involve additional instrumentation. These experiments produce a high data throughput, which can even be dramatically increased by incorporating multiple tones into the driving signal [17]. This accessible and high-throughput experimental technique opens doors to a number of intriguing applications. Here, we have used μMAOS to distinguish the nonlinear mechanical signatures of the cellular cytoplasm from the cortex. The fundamental understanding of cytoplasmic mechanics will lend deeper understanding of biological processes such as mechanotransduction, cancer metastasis, and differentiation, where mechanical behavior of cells plays a critical regulatory role. Other potential applications of μMAOS include data-driven analysis by building large sets of nonlinear microrheological data, and the continuous observation of the nonlinear mechanical response of a material as it changes. Thus, μMAOS stands to become a versatile technique that is essential to future explorations in the physics of soft materials.

ACKNOWLEDGMENTS

We would like to thank Roger D. Kamm, Gareth H. McKinley, and Scott Manalis for helpful discussions. M.G. acknowledges supports from National Institute of General Medical Sciences (Grant No. 1R01GM140108) and the Sloan Research Fellowship. K.R.L. acknowledges the support of the U.S. Department of Energy Computational Science Graduate Fellowship program under Grant No. DE-SC0020347.

[1] R. Mezzenga *et al.*, Nat. Mater. **4**, 729 (2005).
[2] A. Miserez *et al.*, J. Mater. Chem. B **3**, 13 (2015).
[3] M. C. Serrano *et al.*, Adv. Funct. Mater. **20**, 192 (2010).
[4] C. Choi *et al.*, Acc. Chem. Res. **52**, 73 (2018).
[5] M. A. Azad *et al.*, Pharmaceutics **12**, 124 (2020).
[6] T. G. Mason and D. A. Weitz, Phys. Rev. Lett. **74**, 1250 (1995).
[7] M. L. Gardel *et al.*, in *Microscale Diagnostic Techniques* (Springer, Berlin/Heidelberg, 2005), pp. 1–49.
[8] A. Meyer *et al.*, J. Rheology **50**, 77 (2006).
[9] I. Sriram *et al.*, Phys. Fluids **22**, 062003 (2010).
[10] J. R. Gomez-Solano and C. Bechinger, EPL (Europhysics Letters) **108**, 54008 (2014).
[11] J. N. Wilking and T. G. Mason, Phys. Rev. E **77**, 055101(R) (2008).
[12] C. D. Chapman and R. M. Robertson-Anderson, Phys. Rev. Lett. **113**, 098303 (2014).
[13] M. Khan, K. Regan, and R. M. Robertson-Anderson, Phys. Rev. Lett. **123**, 038001 (2019).
[14] J. Hu *et al.*, Proc. Natl. Acad. Sci. **116**, 17175 (2019).
[15] R. H. Ewoldt and N. A. Bharadwaj, Rheol. Acta **52**, 201 (2013).
[16] K. R. Lennon *et al.*, J. Rheology **64**, 551 (2020).
[17] K. R. Lennon *et al.*, J. Rheology **64**, 1263 (2020).
[18] K. Hyun *et al.*, Prog. Polym. Sci. **36**, 1697 (2011).
[19] H. Y. Song and K. Hyun, Korea-Australia Rheology Journal **31**, 267 (2019).
[20] P. K. Singh *et al.*, J. Rheology **62**, 277 (2018).
[21] S. K. Gupta and M. Guo, J. Mech. Phys. Solids **107**, 284 (2017).
[22] S. K. Gupta *et al.*, Soft Matter **15**, 190 (2019).
[23] M.-T. Wei *et al.*, Opt. Express **16**, 8594 (2008).
[24] M.-T. Wei *et al.*, in *Handbook of Photonics for Biomedical Engineering* (Springer, Dordrecht, 2014), pp. 1–20.
[25] R. Brau *et al.*, Journal of Optics A: Pure and Applied Optics **9**, S103 (2007).
[26] V. Volterra, *Theory of Functionals and of Integral and Integro-differential Equations* (Dover, New York, 1959).
[27] M. A. Joens and J. W. Swan, arXiv:2106.7774.
[28] J. Mohanty, A. C. Bhasikuttan, S. D. Choudhury, and H. Pal, J. Phys. Chem. B **112**, 10782 (2008).
[29] F. Nettesheim and N. J. Wagner, Langmuir **23**, 5267 (2007).
[30] H. Rehage and H. Hoffmann, Mol. Phys. **74**, 933 (1991).
[31] T. Shikata, S. J. Dahman, and D. S. Pearson, Langmuir **10**, 3470 (1994).
[32] M. T. Valentine, Z. E. Perlman, M. L. Gardel, J. H. Shin, P. Matsudaira, T. J. Mitchison, and D. A. Weitz, Biophys. J. **86**, 4004 (2004).
[33] M. Guo *et al.*, Cell **158**, 822 (2014).
[34] B. R. Daniels, B. C. Masi, and D. Wirtz, Biophys. J. **90**, 4712 (2006).
[35] S. Mahammad, S. Murthy, A. Didonna, B. Grin, E. Israeli, R. Perrot, P. Bomont, J. Julien, E. Kuczmarski, P. Opal, and R. Goldman, J. Clin. Invest. **123**, 1964 (2013).
[36] M. L. Gardel *et al.*, Proc. Natl. Acad. Sci. **103**, 1762 (2006).
[37] K. R. Lennon *et al.*, arXiv:2104.11040.
[38] H. Huang *et al.*, American Journal of Physiology-Cell Physiology **287**, C1 (2004).
[39] A. Malandrino *et al.*, ACS Biomaterials Science & Engineering **4**, 294 (2018).
[40] Y. Li *et al.*, Cell Stem Cell **28**, 63 (2021).
[41] F. Chowdhury *et al.*, Nat. Mater. **9**, 82 (2010).
[42] M. Guo *et al.*, Proc. Natl. Acad. Sci. **114**, E8618 (2017).
[43] B. Fabry, G. N. Maksym, J. P. Butler, M. Glogauer, D. Navajas, and J. J. Fredberg, Phys. Rev. Lett. **87**, 148102 (2001).
[44] P. Kollmannsberger and B. Fabry, Annu. Rev. Mater. Res. **41**, 75 (2011).
[45] P. Kollmannsberger *et al.*, Soft Matter **7**, 3127 (2011).
[46] P. Fernández *et al.*, Biophys. J. **90**, 3796 (2006).
[47] T. P. Stossel, The Journal of Cell Biology **99**, 15s (1984).

[48] M. Guo *et al.*, Biophys. J. **105**, 1562 (2013).
[49] J. Stricker, T. Falzone, and M. L. Gardel, J. Biomech. **43**, 9 (2010).
[50] H. Lee, J. M. Ferrer, M. J. Lang, and R. D. Kamm, Phys. Rev. E **82**, 011919 (2010).
[51] S. Hurst *et al.*, bioRxiv (2021).
[52] C. Duclut, J. Paijmans, M. M. Inamdar, C. D. Modes, and F. Jülicher, arXiv:2103.16462.
[53] O. Arnolds *et al.*, Rheol. Acta **49**, 1207 (2010).
[54] T. B. Goudoulas and N. Germann, J. Rheology **62**, 1299 (2018).